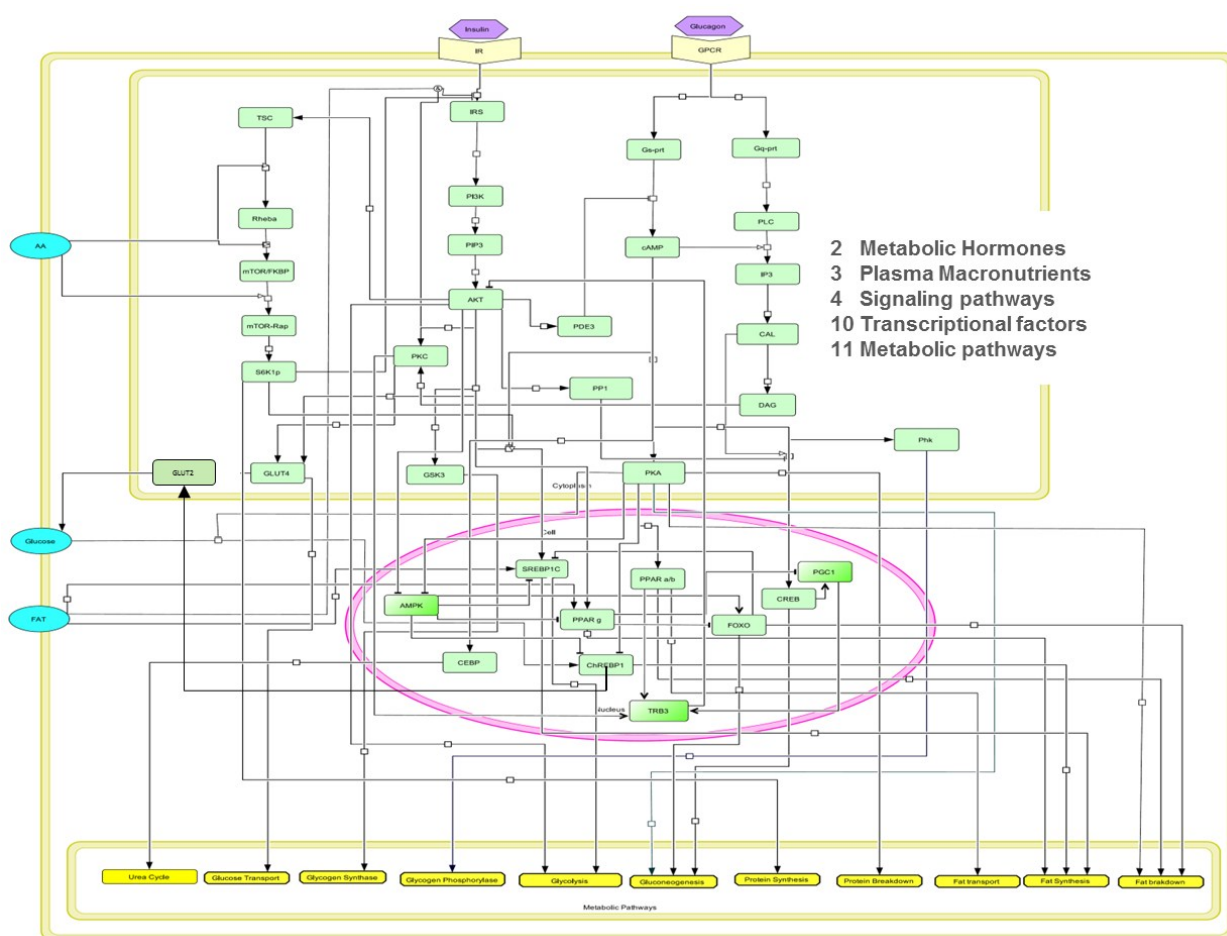
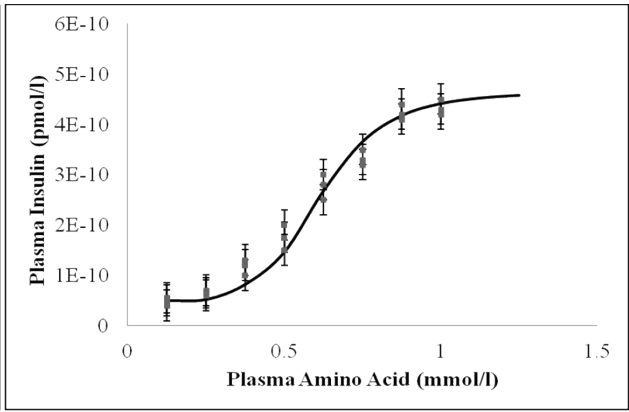
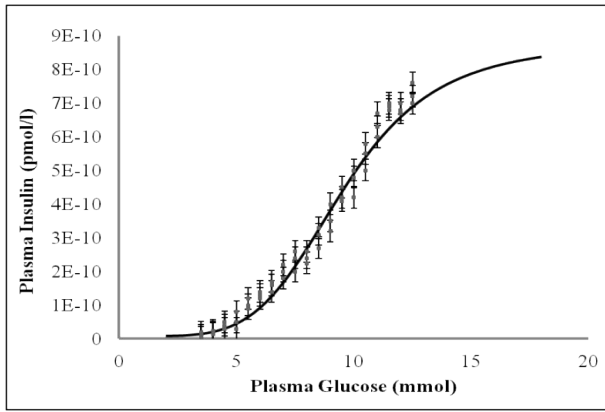


1 Supplementary File 1-

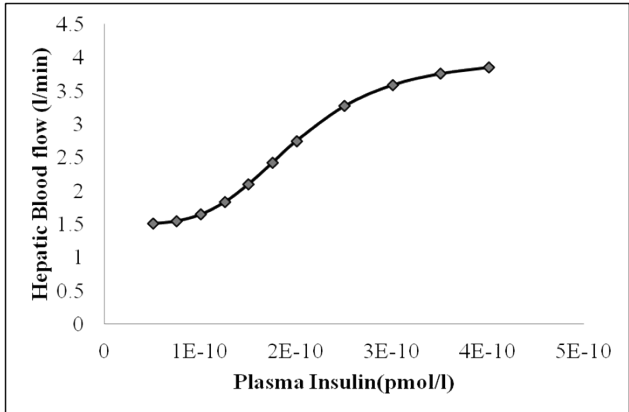
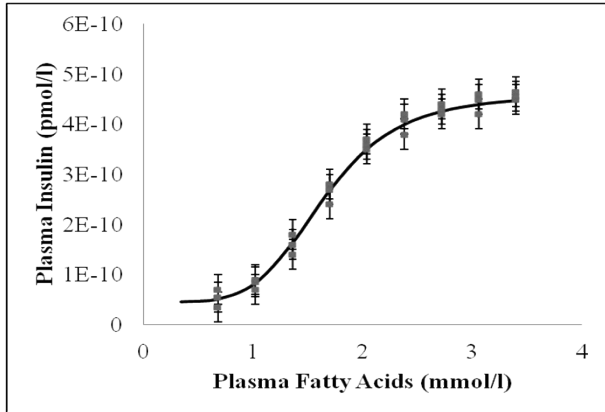


2

3 **Figure 1***- The detailed molecular regulatory network comprising of the interactions between 2
 4 metabolic hormones (insulin and glucagon), 3 macronutrients (glucose, amino acids and fatty
 5 acids), 4 signaling pathways (insulin signaling, mTOR signaling, Glucagon signaling and
 6 calcium signaling) along with major metabolic transcriptional factors and metabolic pathways.



7



8

9 **Figure M1** The Hill fit curves for the data from literature reported for the plasma insulin levels
 10 with respect to (A) Plasma Glucose, (B) Plasma Amino Acids, (C) Plasma Fatty acids and (D)
 11 Blood flow with respect to plasma insulin levels.

12

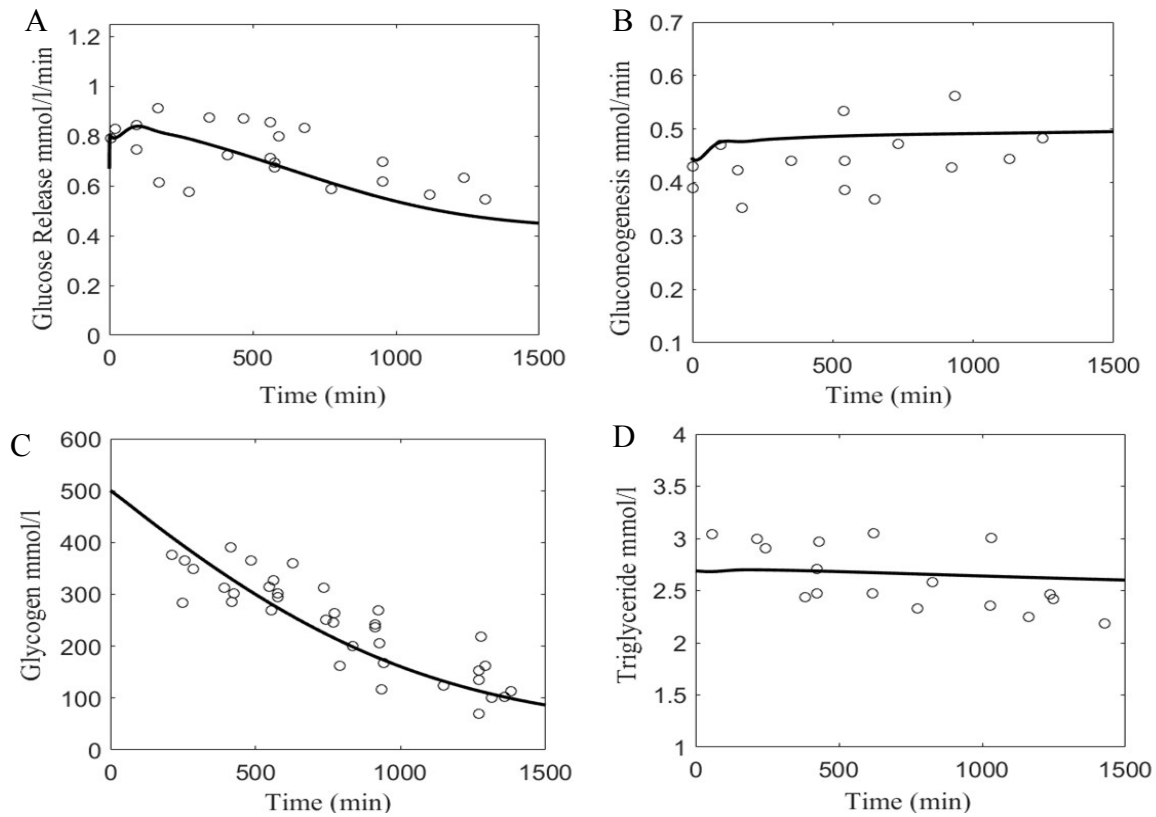
13

14

15

16

17



18

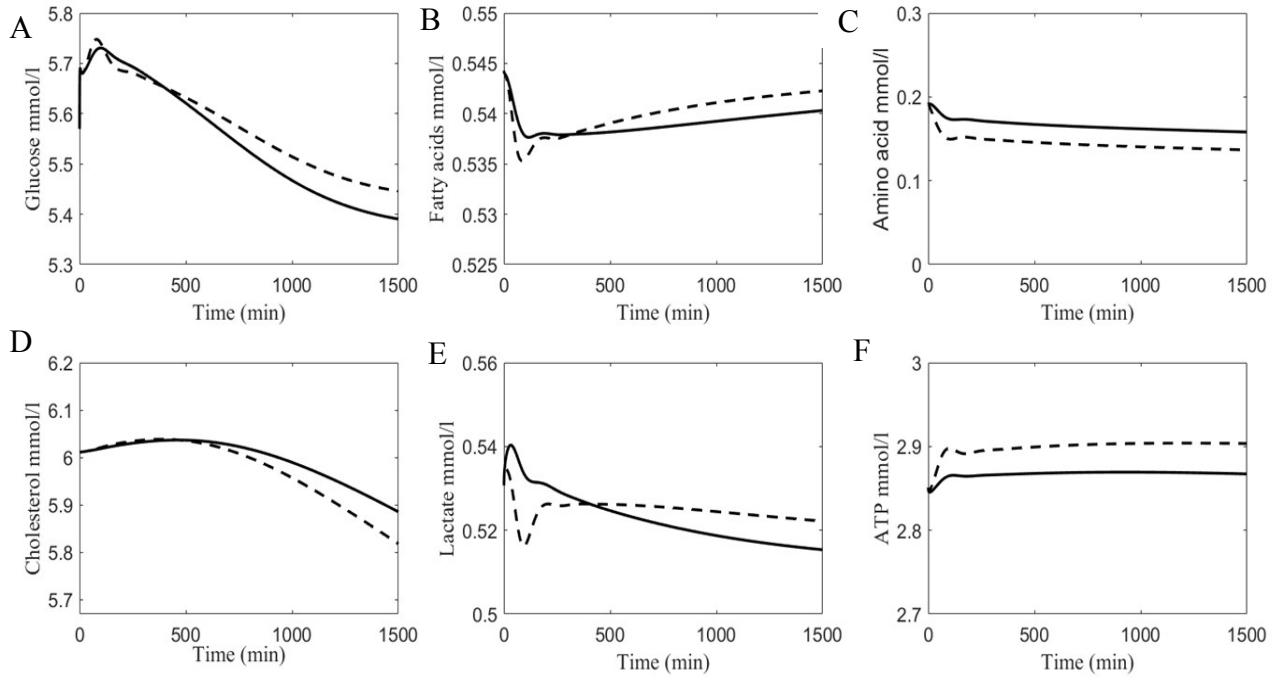
19 **Figure M2 (I)** Validation of fluxes and metabolite profiles in liver for resting state. The solid line
 20 represents simulation profile and the 'o' markers represent the experimental data. (A) Hepatic
 21 glucose release profile validated with the data reported by Konig et al. 2012¹, Edgerton et al
 22 2006² and Meyer et al 1998³ (B) Gluconeogenesis profile validated with data reported in Konig et
 23 al 2012¹ and Edgerton et al 2006² (C) Glycogen profile validated with data reported in Konig et al
 24 2012¹ (D) Triglycerides profile validated with data reported in Ferrell and Chiang et al. 2015⁴ and
 25 Ravi Kumar et al. 2004⁵.

26

27

28

29



31

32 **Figure M2(II)** Validation of resting hepatic metabolite profiles with the source models (Konig et
 33 al 2012¹ and Xu et al 2011⁶). The solid line represents the simulation results and the dashed line
 34 represents the simulation profiles by the source models.

35

36

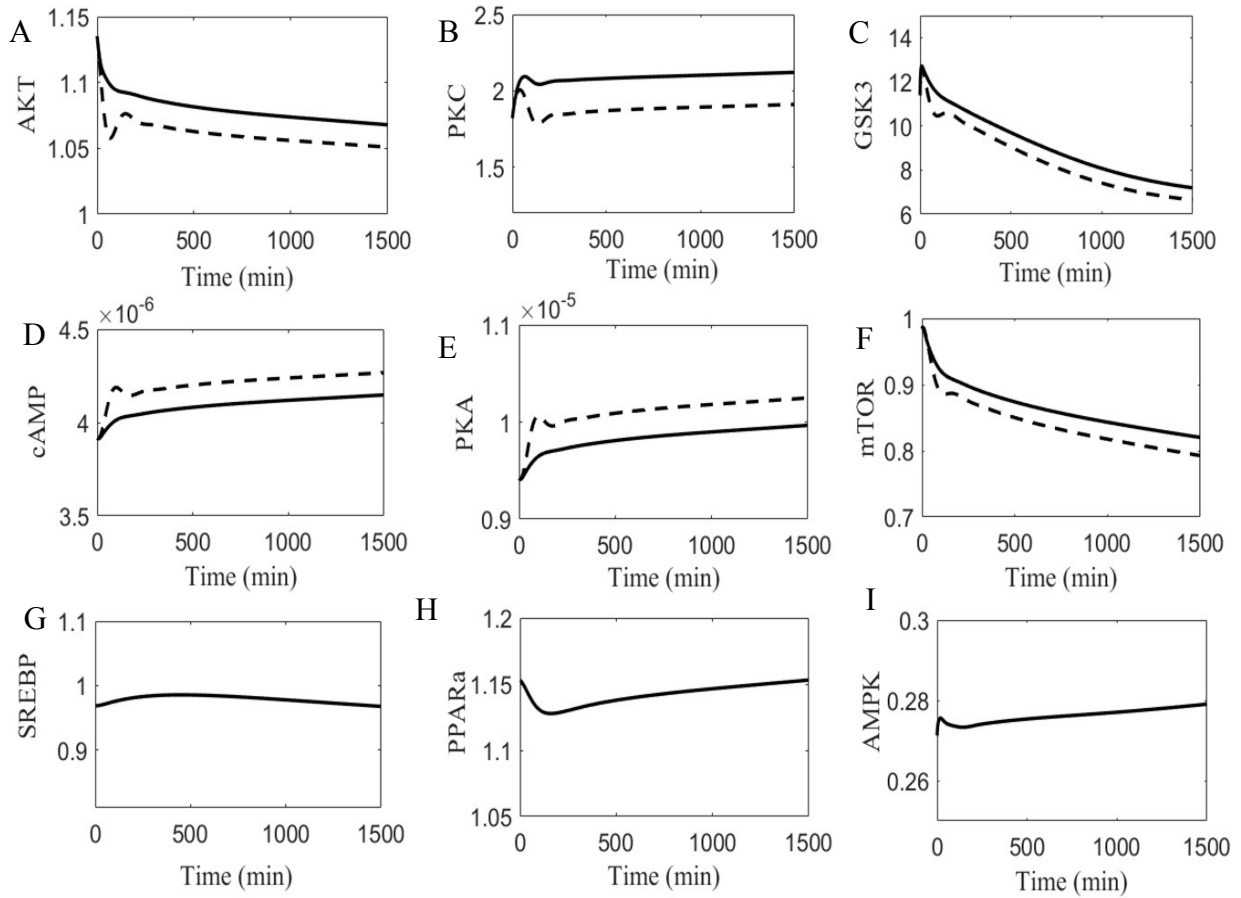
37

38

39

40

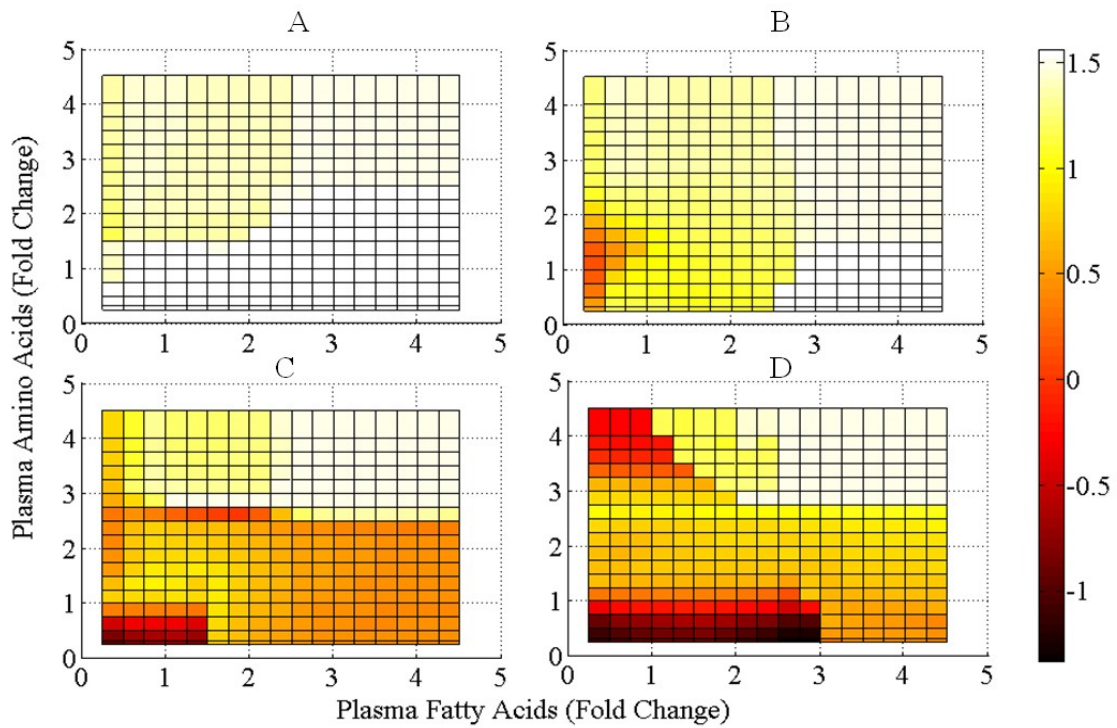
41



43

44 **Figure M2(III)** Validation of Signaling and transcriptional profiles in liver while resting state
 45 with the source models. The solid line represents the simulation results and the dashed line
 46 represents the simulation profiles by the source models. The signaling components were validated
 47 by model profiles from Sedaghat et al 2002⁷ for AKT and PKC, Mutalik et al 2007⁸ and Xu et al
 48 2011⁶ for GSK3, cAMP and PKA, Vinod and Venkatesh 2009⁹ for mTOR. The transcription
 49 model represents the qualitative trends and the fold changes based upon the data reported in
 50 literature (refer to transcription module in methodology section).

51



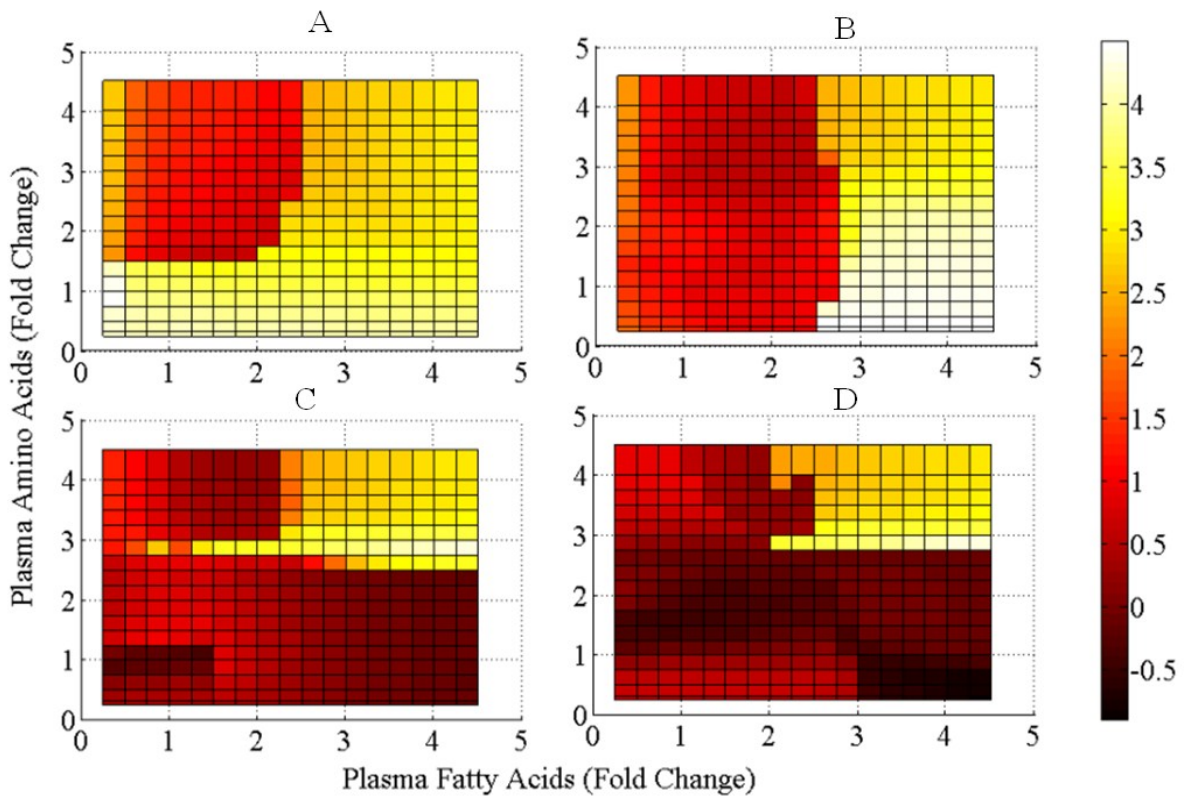
52

53 **Figure M3** The pyruvate transport flux for varying levels of plasma amino and fatty acids for
 54 four different glucose conditions. A positive value on the color bar represents the pyruvate
 55 uptake into the plasma from the liver, whereas a negative value represents the release of the
 56 pyruvate by hepatic tissues.

57

58

59

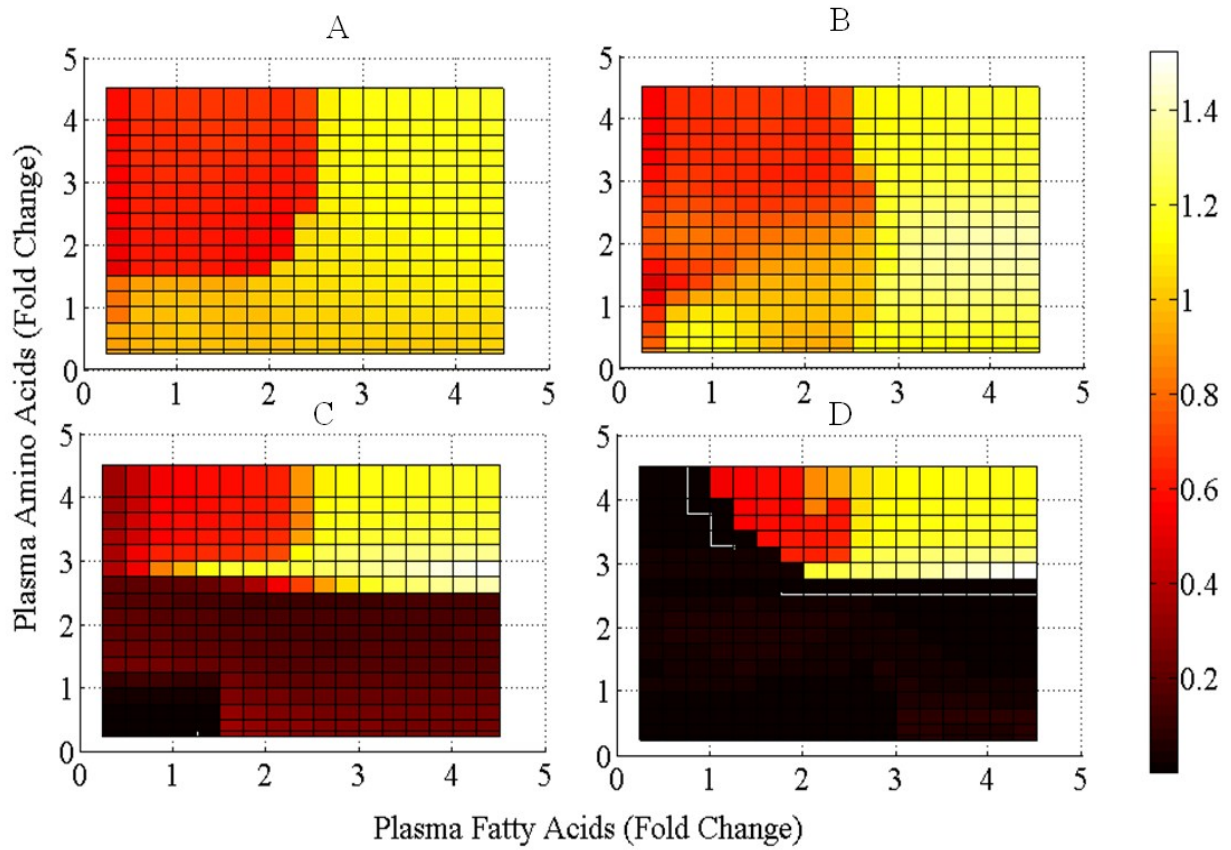


60

61 **Figure M4** The Lactate transport flux varying levels of plasma amino and fatty acids for four
 62 different glucose conditions. A positive value on the color bar represents the lactate uptake into
 63 the plasma from the liver, whereas a negative value represents the release of the lactate by
 64 hepatic tissues.

65

66



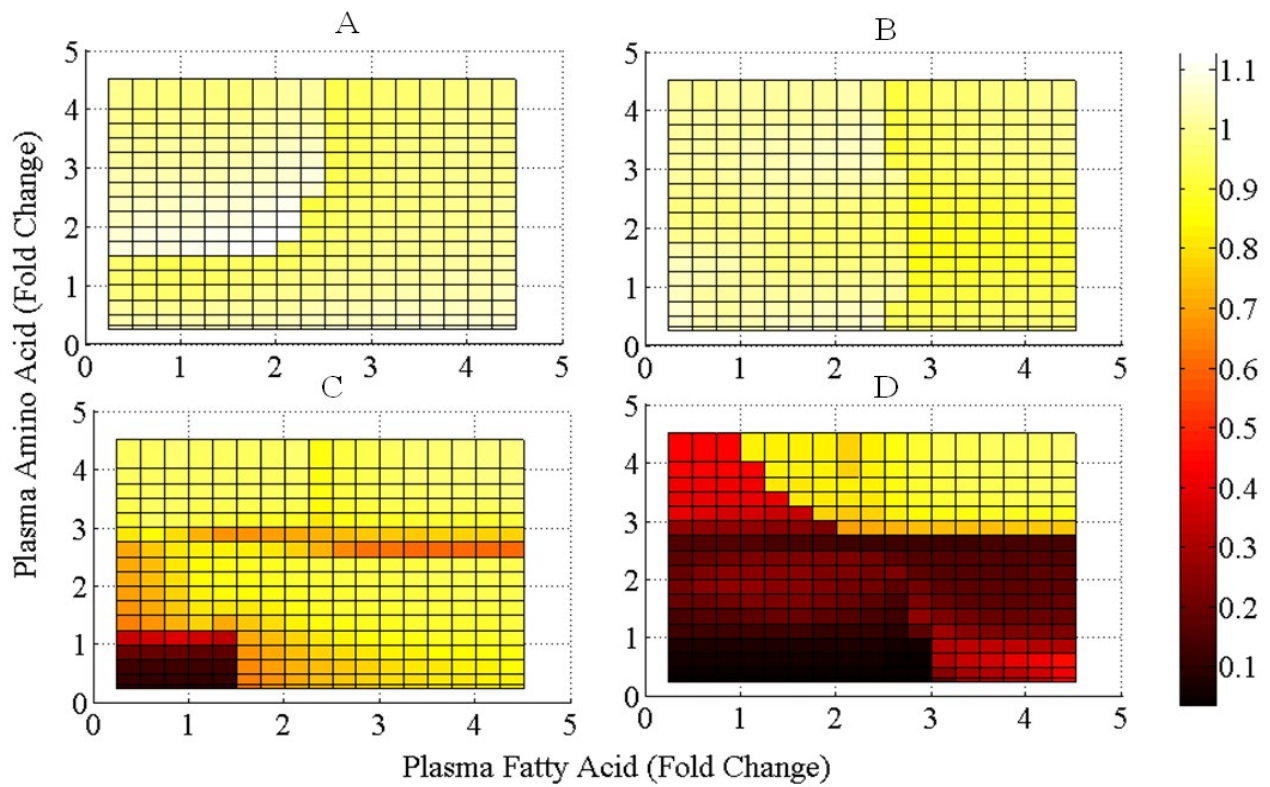
67

68 **Figure M5** Thepyruvate carboxylase flux varying levels of plasma amino and fatty acids for
 69 four different glucose conditions.

70

71

72

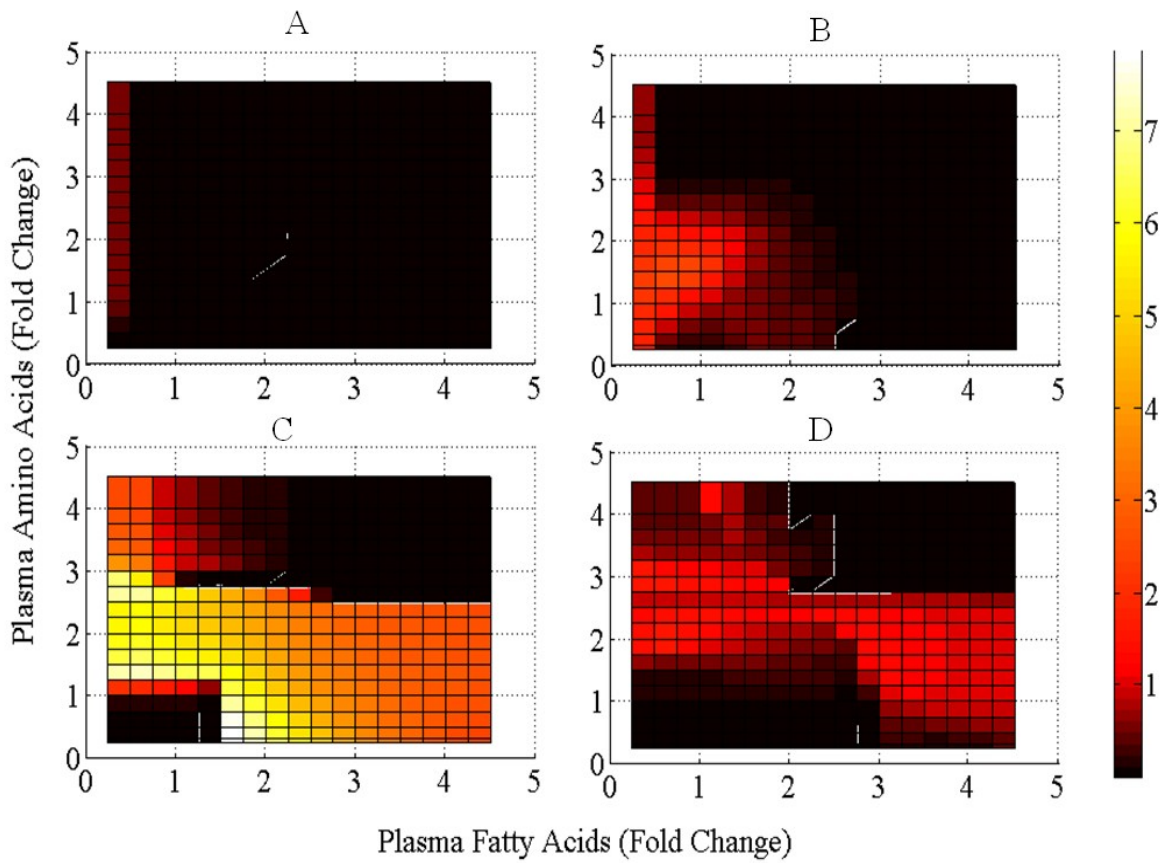


73

74 **Figure M6** Theratio of ATP breakdown [Adenylate kinase flux] to ATP production (oxidative
 75 phosphorylation flux) for varying levels of plasma amino and fatty acids for four different
 76 glucose conditions. The ratio below one represents that the ATP production flux is higher than
 77 the ATP lysis flux.

78

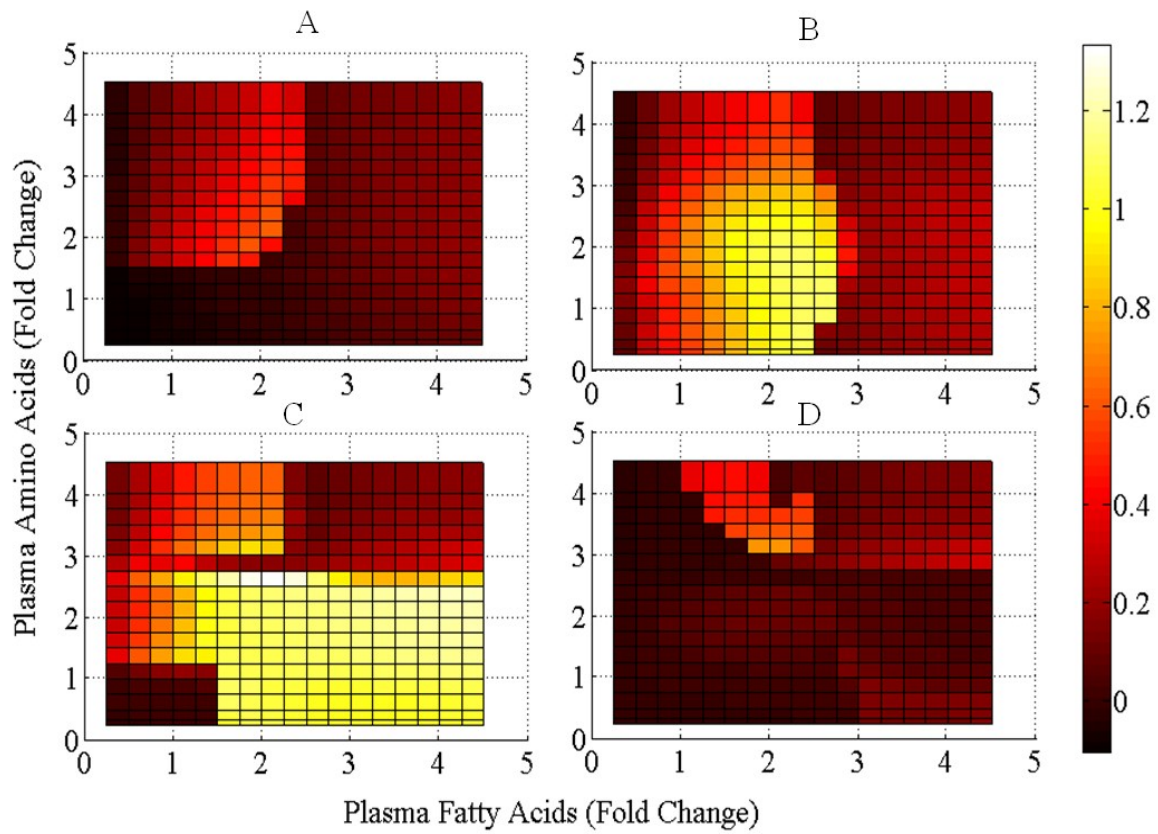
79



80

81 **Figure M7** Therate of pentose phosphate pathway represented Glucose 6 phosphate
 82 dehydrogenase flux that is abstracted for conversion of G6p to ribulose 5 phosphate for varying
 83 levels of plasma amino and fatty acids for four different glucose conditions.

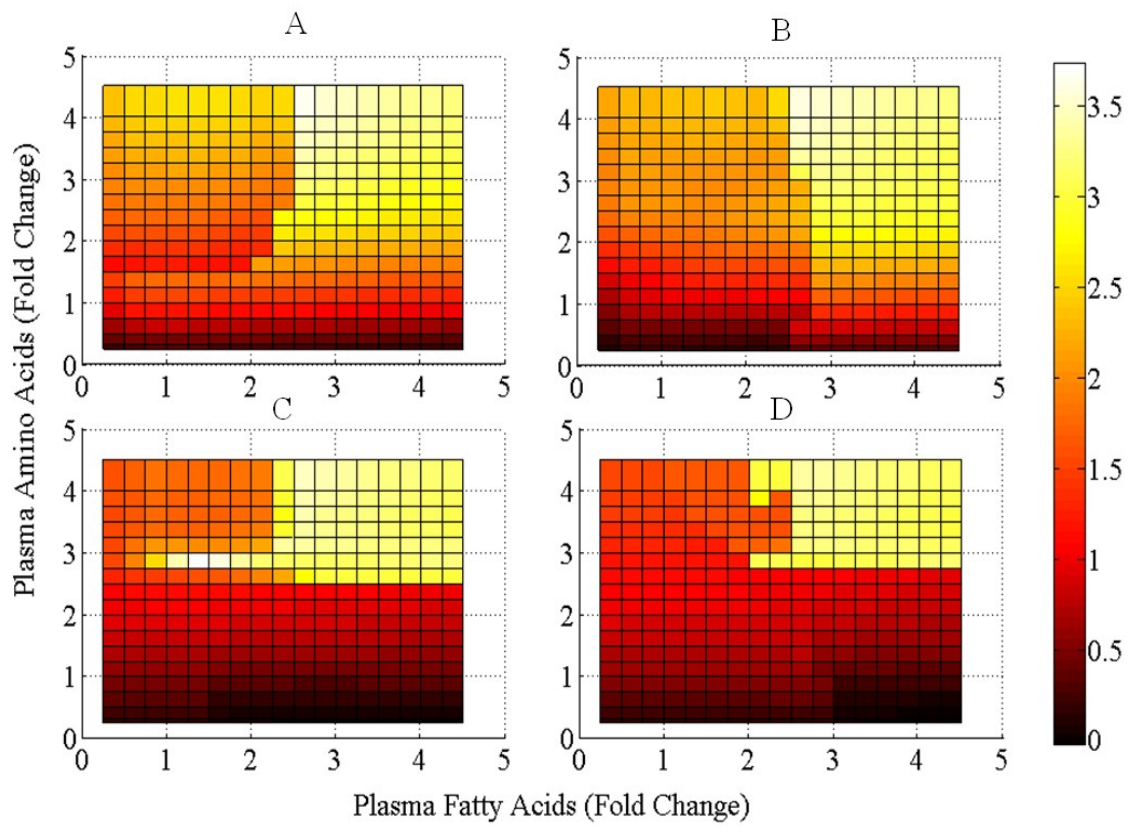
84



85

86 **Figure M8** The triglyceride transport flux for varying levels of plasma amino and fatty acids for
 87 four different glucose conditions. The value below one represents the net flux is towards
 88 triglyceride release and vice versa.

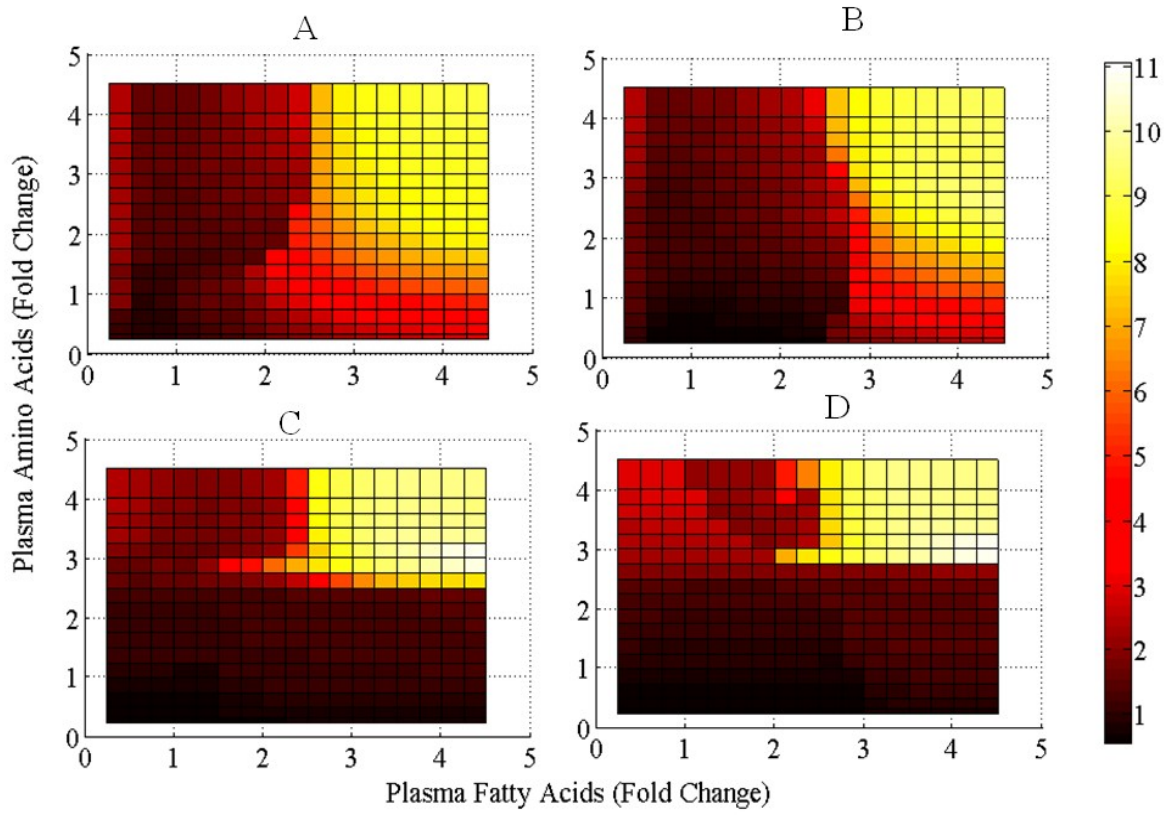
89



90

91 **Figure M9** The Amino acid uptake flux from the liver, for varying levels of plasma amino and
 92 fatty acids for four different glucose conditions.

93



94

95 **Figure M10** The steady state fold change in ammonia levels in liver for varying levels of
 96 plasma amino and fatty acids for four different glucose conditions.

97

98

99

100

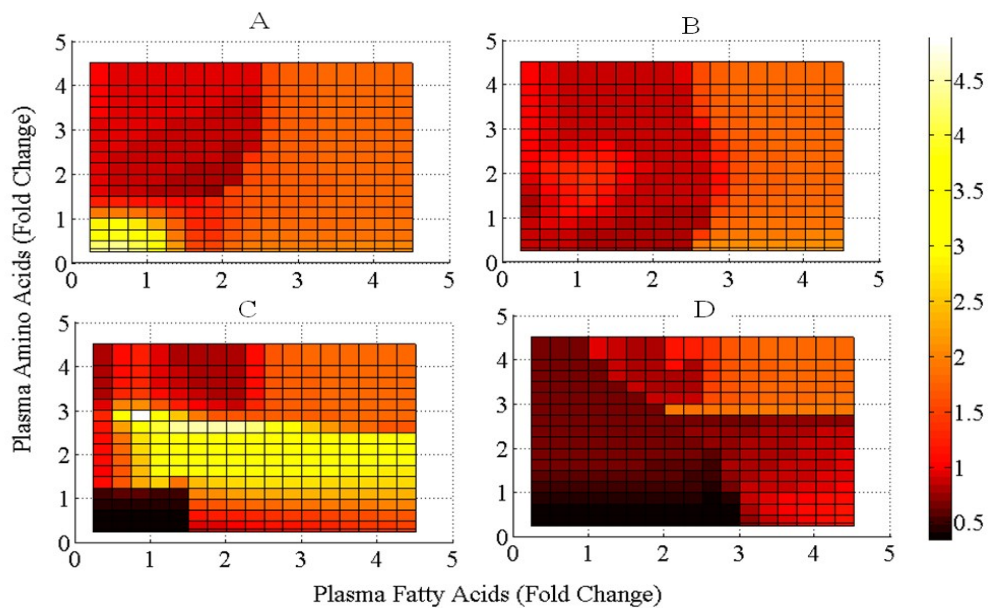
101

102

103

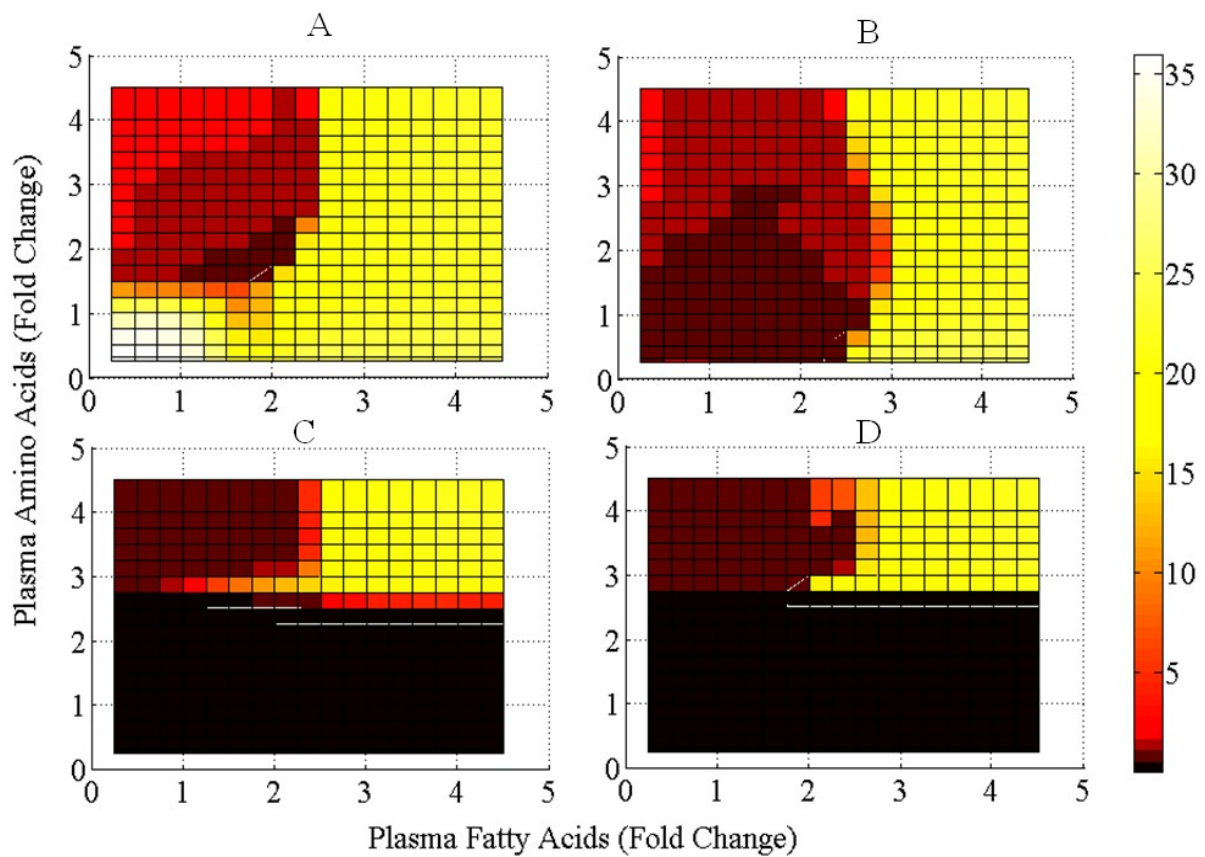
104 Steady States of Signaling and Transcription factors

105 Steady state responses for some of the key signaling regulators and transcription factors with
106 respect of varying levels of amino acids and fatty acids for four different glucose levels [low,
107 normal, moderately high, very high] are shown in the Figures below [Fig..S1 to Fig..S12]. The
108 trends observed in the above mentioned metabolic fluxes are resultant effects of the states of
109 signaling and transcriptional molecules. AKT, mTOR, S6K1p, CHREBP, SREBP and PPAR γ
110 are the anabolic regulators activated by glucose, insulin, amino acids and fatty acids. PKA, PKC,
111 AMPK, FOXO, PPAR α and TRB3 are the catabolic regulators activated by the glucagon, amino
112 acids and fatty acids. The interplay of these regulators at signaling and transcriptional levels
113 under different dietary conditions yield the specific metabolic state of the tissue. These metabolic
114 states decide upon the healthy or disease condition of the tissue.



115

116 **Figure N1** The steady state response of AKT phosphorylation for varying levels of plasma amino and
117 fatty acids for four different glucose conditions. AKTp increases with increasing glucose levels and
118 decreases with increasing amino and fatty acid levels. AKTp is highest at high glucose and low amino
119 fatty acid conditions and lowest at very high amino fatty acid conditions.



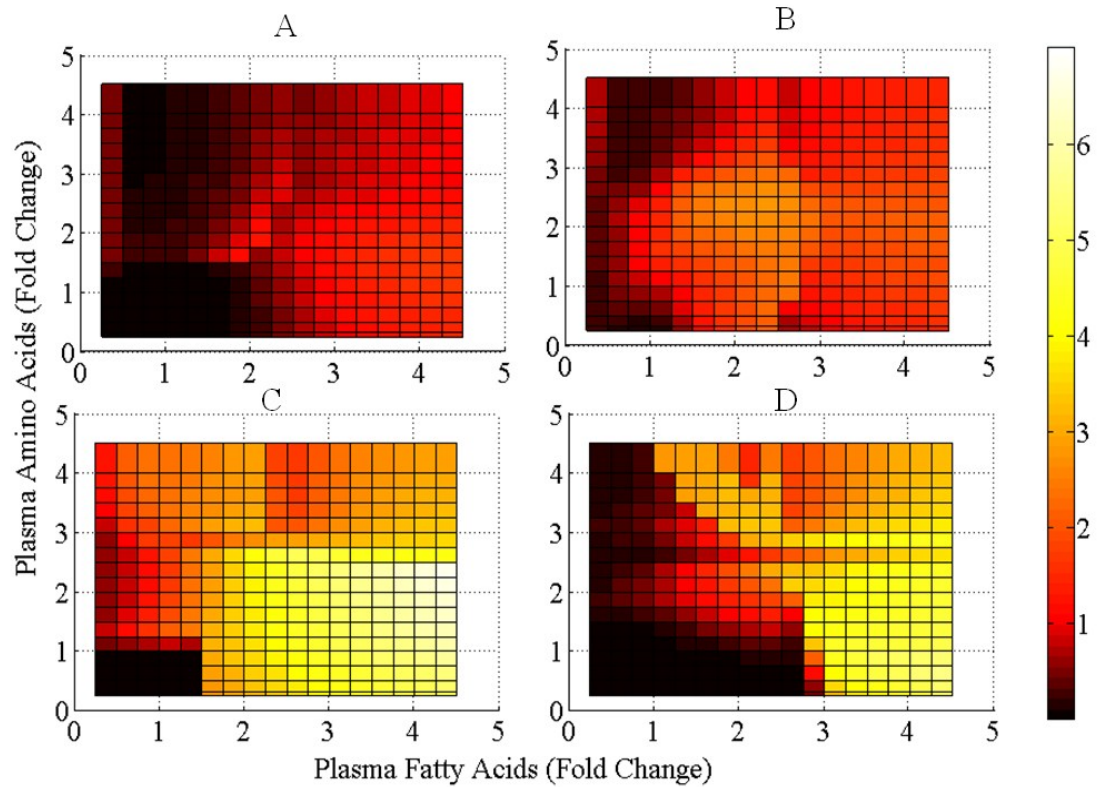
120

121 **Figure N2** The steady state response of PKA activation for varying levels of plasma amino and
 122 fatty acids for four different glucose conditions. PKA increases with increasing amino and fatty
 123 acid levels and decreases with increasing glucose levels. PKA is highest at low glucose and low
 124 amino fatty acid conditions and lowest at very high glucose conditions.

125

126

127



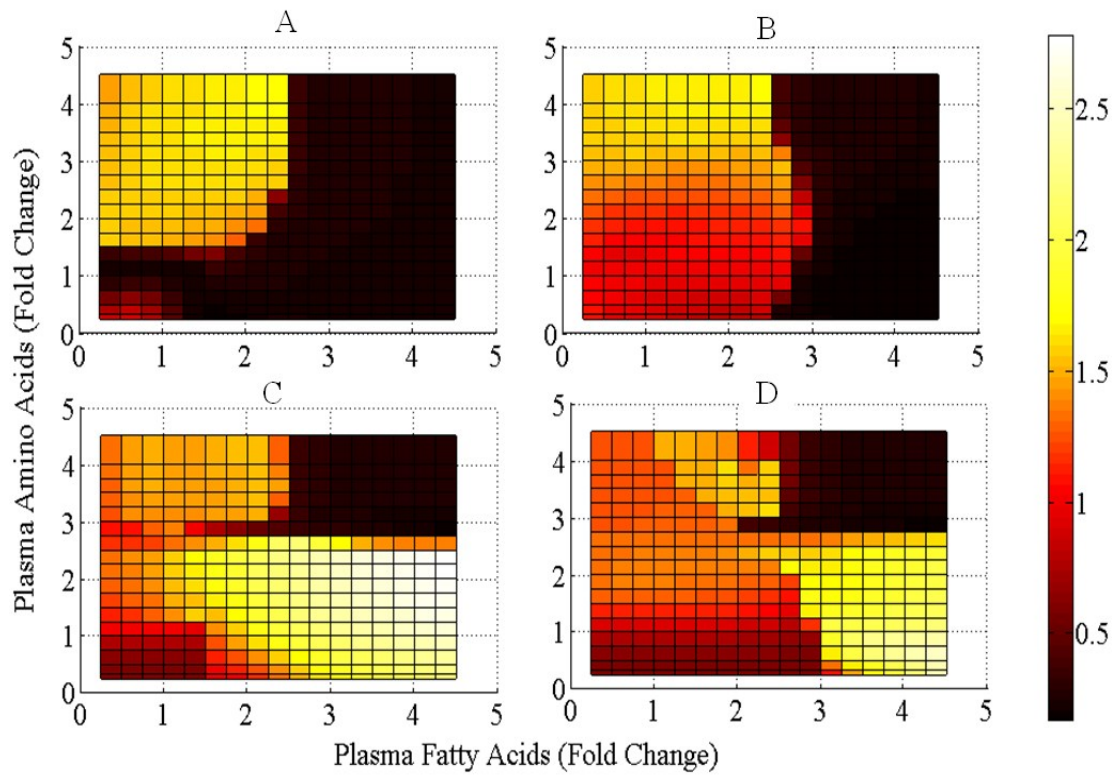
128

129 **Figure N3** The steady state response of PKC activation for varying levels of plasma amino and
 130 fatty acids for four different glucose conditions. PKC increases with increasing glucose and fatty
 131 acid levels and decreases with increasing amino acid levels. However under high glucose
 132 conditions, it increases with fatty acid levels and decreases with decreasing fatty acids.

133

134

135

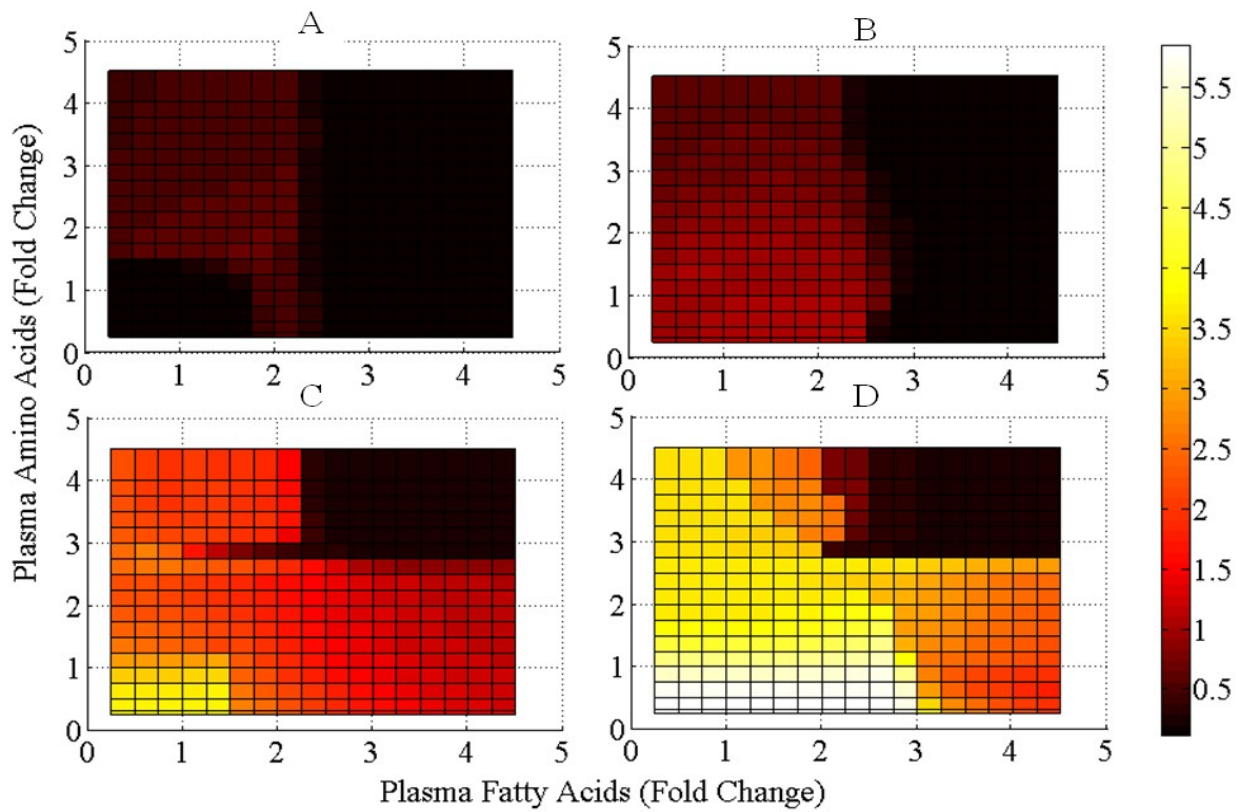


136

137 **Figure N4** The steady state response of AMPK activation for varying levels of plasma amino
 138 and fatty acids for four different glucose conditions. AMPK increases with low glucose and high
 139 amino acid levels and decreases with increasing fatty acid levels. However, under high glucose
 140 condition it increases with increasing fatty acids and decreases with lower amino acid levels. It is
 141 mostly inhibited at high amino fatty acid levels.

142

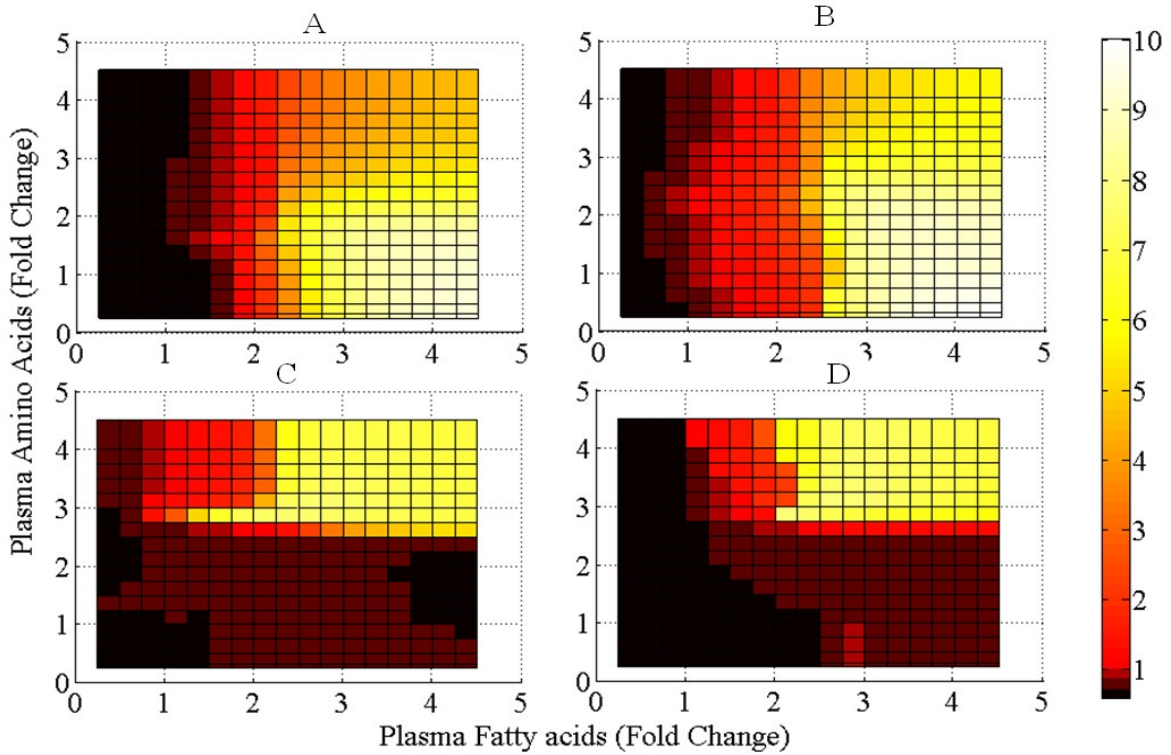
143



144

145 **Figure N5** The steady state response of CHREBP activation for varying levels of plasma amino
 146 and fatty acids for four different glucose conditions. CHREBP increases with increasing glucose
 147 and decreases with increasing fatty acids at normal glucose levels, due to inhibition of AKT. It is
 148 inhibited at high amino fatty acid levels.

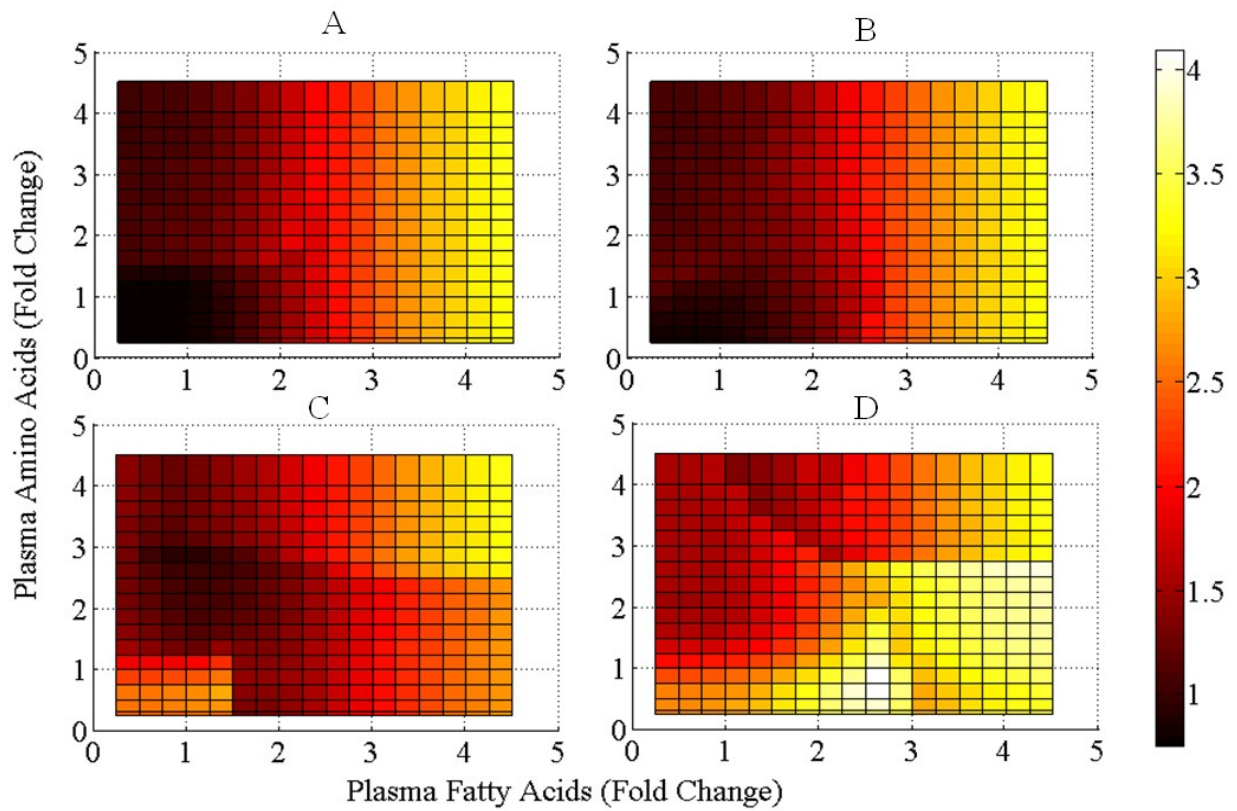
149



150

151 **Figure N6** The steady state response of TRB3 activation for varying levels of plasma amino and
 152 fatty acids for four different glucose conditions. TRB3 increases with increasing Fatty acids and
 153 decreases with increasing glucose levels. However at lower glucose levels it also decreases with
 154 increasing amino acid levels, whereas, at higher glucose levels, it increases with increasing
 155 amino fatty acids.

156

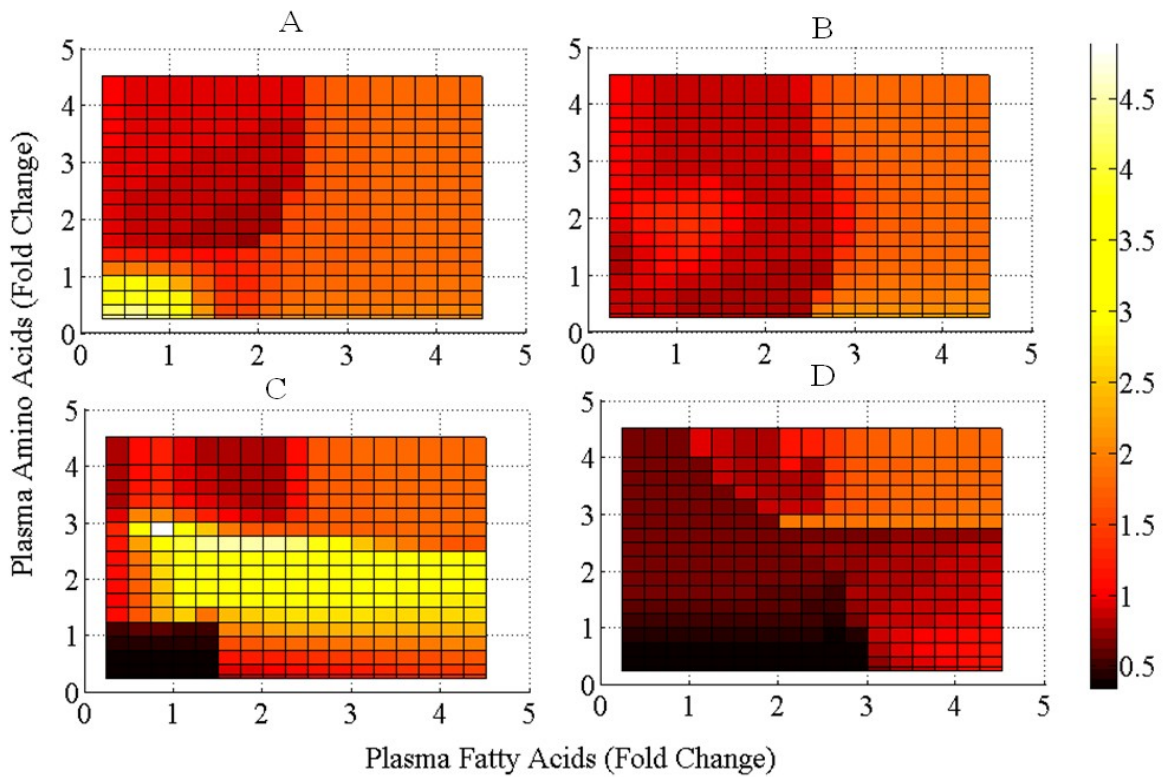


157

158 **Figure N7** The steady state response of PPAR γ activation for varying levels of plasma amino and
 159 fatty acids for four different glucose conditions. PPAR γ expression increases with increasing
 160 fatty acid levels. Under normal glucose levels, it is inhibited at low amino acid and low fatty acid
 161 and at high glucose condition it is reduced with increasing amino acid levels.

162

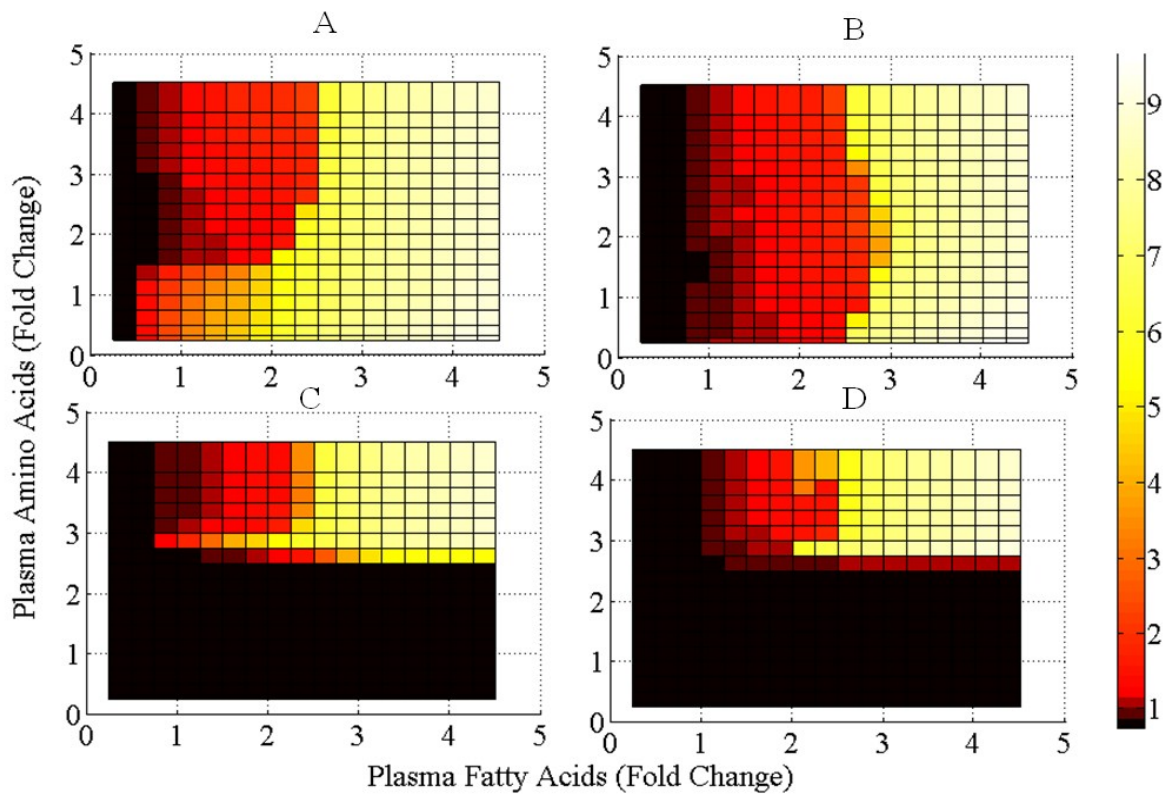
163



164

165 **Figure N8** The steady state response of FOXO activation for varying levels of plasma amino
 166 and fatty acids for four different glucose conditions. FOXO increases at very low glucose fat
 167 amino acid condition. At normal glucose levels it increases with high fatty acid levels. At high
 168 glucose levels, it is highest at moderate amino acids conditions. However at very high glucose,
 169 its activation decreases due to increasing levels of AMPK and PPAR γ that are inhibitors of
 170 FOXO.

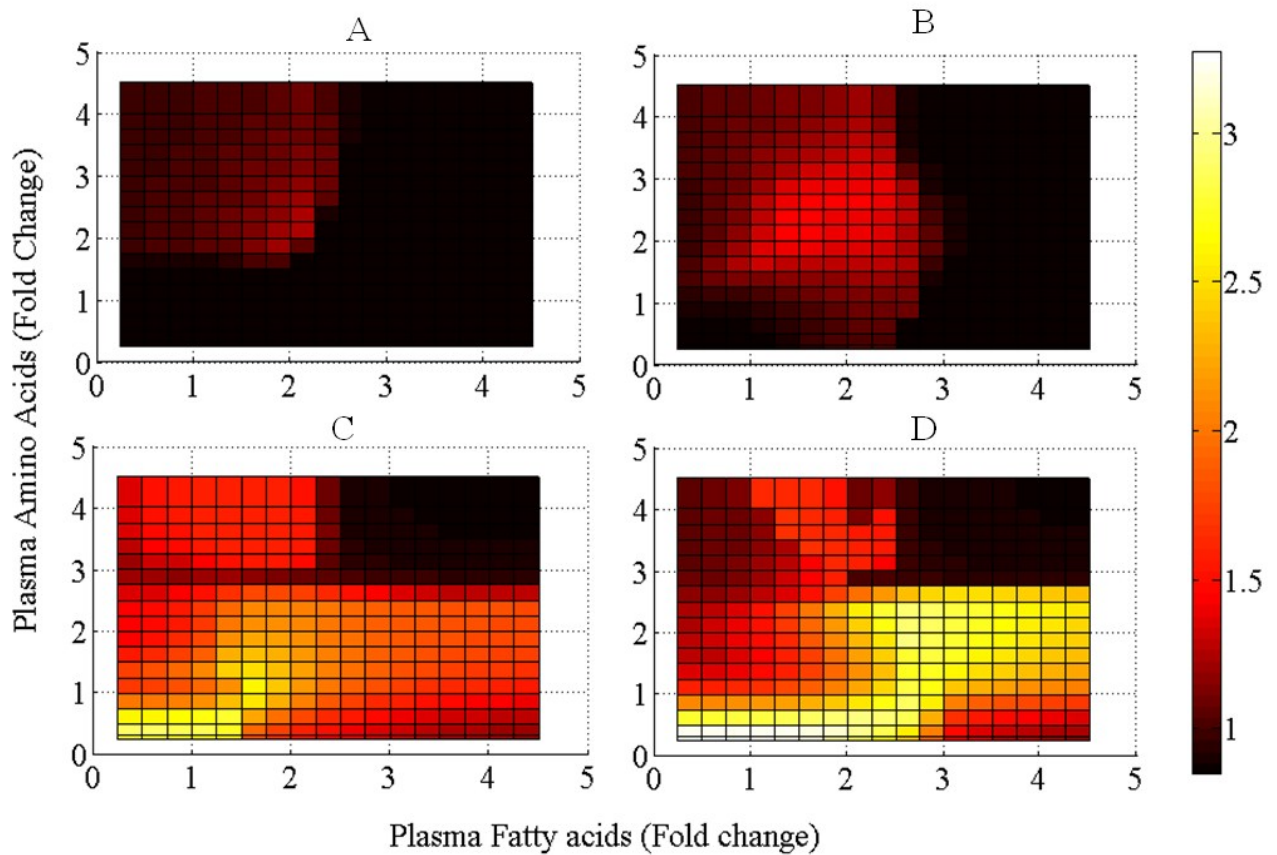
171



172

173 **Figure N9** The steady state response of PPAR α activation for varying levels of plasma amino
 174 and fatty acids for four different glucose conditions. It increases with increasing fatty acid levels
 175 and decreases with increasing glucose levels. However under high glucose levels it increases
 176 with high amino fatty acid condition. PPAR α is activated by fatty acids and PKA and deactivated
 177 by AKT.

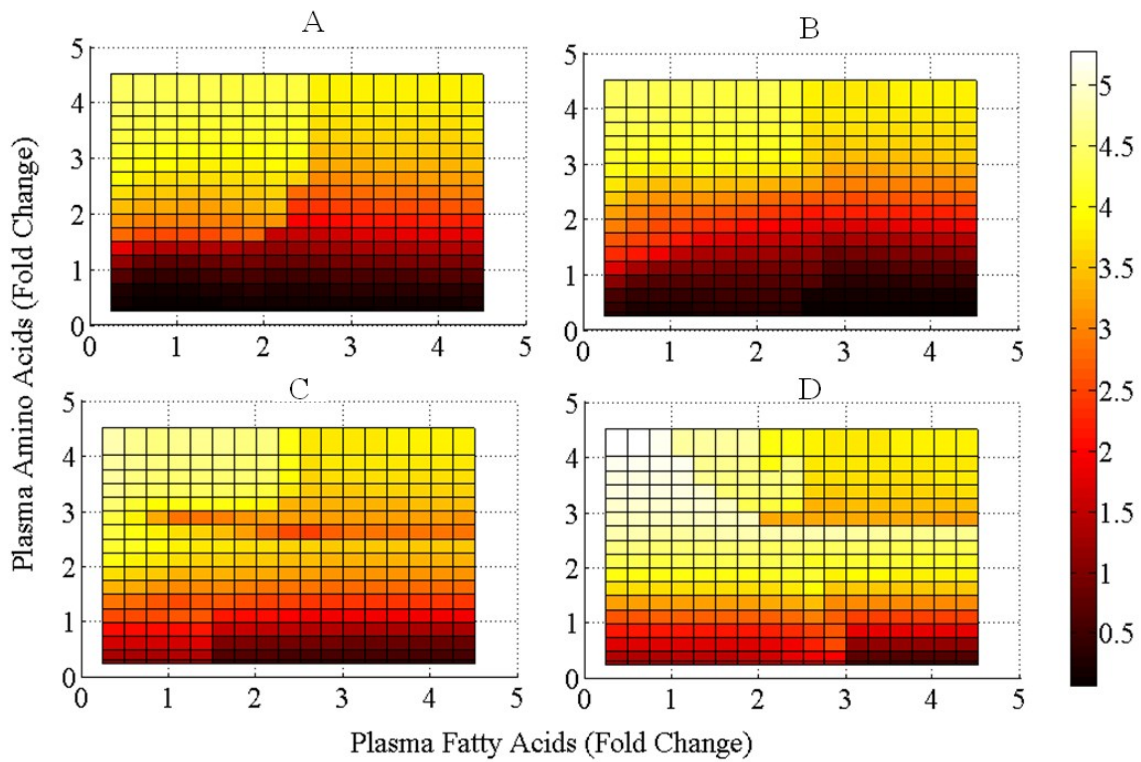
178



179

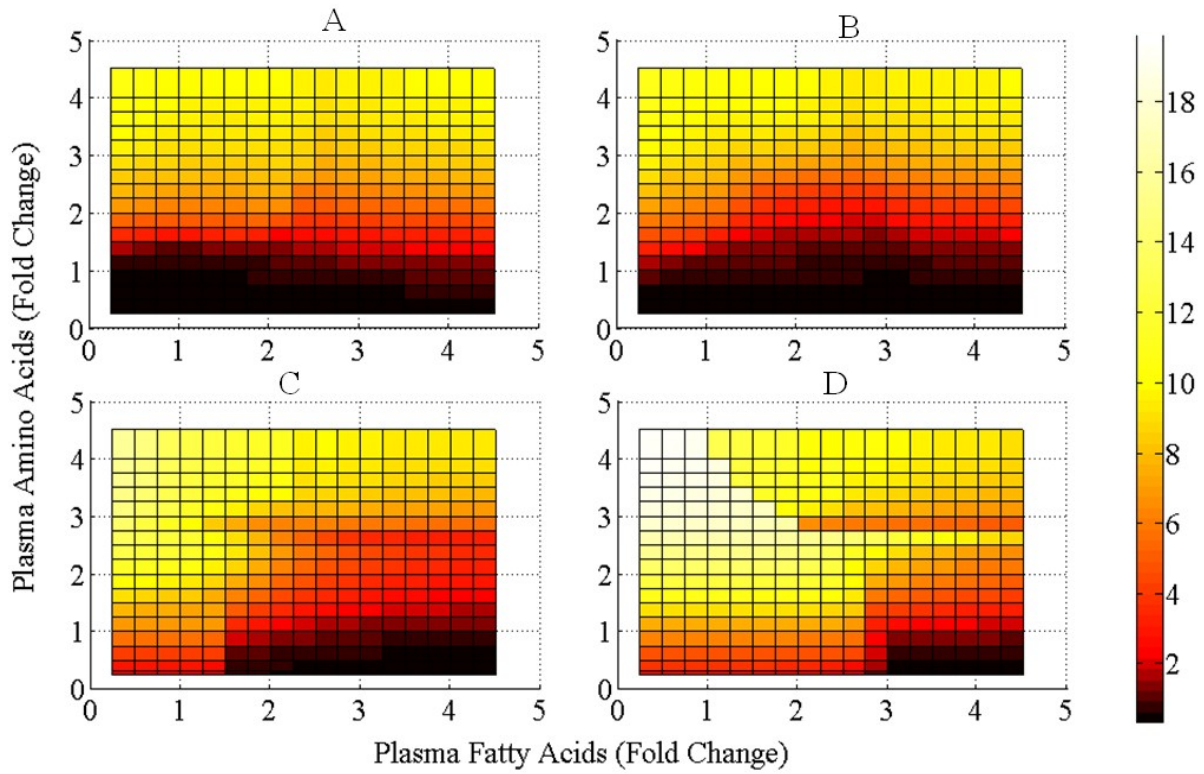
180 **Figure N10** The steady state response of SREBP activation for varying levels of plasma amino
 181 and fatty acids for four different glucose conditions. SREBP increases with increasing amino
 182 acid and decreasing fatty acid conditions under normal glucose levels. However, it is contrast
 183 under high glucose conditions.

184



185

186 **Figure N11** The steady state response of mTOR activation for varying levels of plasma amino and
 187 fatty acids for four different glucose conditions. mTOR increases with increasing amino acid and
 188 glucose levels and decreases with lower amino acid levels. The Figure shows sensitivity of
 189 mTOR to amino acids decrease with increasing fatty acid levels. Therefore, it is highest at high
 190 amino glucose and low fatty acid condition.



191

192 **Figure N12** The steady state response of S6K phosphorylation for varying levels of plasma
 193 amino and fatty acids for four different glucose conditions. This follows the trend similar to
 194 mTOR.

195

196

197

198

199

200

201

202

203

204 **References**

- 205 1. Konig, M. & Holzhutter, H.-G. Kinetic Modeling of Human Hepatic Glucose Metabolism in
206 Type 2 Diabetes Mellitus Predicts Higher Risk of Hypoglycemic Events in Rigorous Insulin
207 Therapy. *J. Biol. Chem.***287**, 36978–36989 (2012).
- 208 2. Edgerton, D. S. Insulin’s direct effects on the liver dominate the control of hepatic glucose
209 production. *J. Clin. Invest.***116**, 521–527 (2006).
- 210 3. Meyer, C., Dostou, J., Nadkarni, V. & Gerich, J. Effects of physiological hyperinsulinemia on
211 systemic, renal, and hepatic substrate metabolism. *Am. J. Physiol.-Ren. Physiol.***275**, F915–
212 F921 (1998).
- 213 4. Ferrell, J. M. & Chiang, J. Y. Short-term circadian disruption impairs bile acid and lipid
214 homeostasis in mice. *CMGH Cell. Mol. Gastroenterol. Hepatol.***1**, 664–677 (2015).
- 215 5. Ravikumar, B. Real-time assessment of postprandial fat storage in liver and skeletal muscle in
216 health and type 2 diabetes. *AJP Endocrinol. Metab.***288**, E789–E797 (2004).
- 217 6. Xu, K., Morgan, K. T., Todd Gehris, A., Elston, T. C. & Gomez, S. M. A Whole-Body Model
218 for Glycogen Regulation Reveals a Critical Role for Substrate Cycling in Maintaining Blood
219 Glucose Homeostasis. *PLoS Comput. Biol.***7**, e1002272 (2011).
- 220 7. Sedaghat, A. R., Sherman, A. & Quon, M. J. A mathematical model of metabolic insulin
221 signaling pathways. *Am. J. Physiol. - Endocrinol. Metab.***283**, E1084–E1101 (2002).
- 222 8. Mutalik, V. K. & Venkatesh, K. V. Quantification of the glycogen cascade system: the
223 ultrasensitive responses of liver glycogen synthase and muscle phosphorylase are due to
224 distinctive regulatory designs. *Theor. Biol. Med. Model.***2**, 19 (2005).
- 225 9. Vinod, P. K. U. & Venkatesh, K. V. Quantification of the effect of amino acids on an
226 integrated mTOR and insulin signaling pathway. *Mol. Biosyst.***5**, 1163 (2009).
- 227